Journal of Marine Technology and Environment
DOI:10.53464/JMTE.02.2026.02
ISSN (Print): 1844-6116
ISSN (Online): 2501-8795
https://www. jmte.eu

COMPUTATIONAL ANALYSIS OF PARAMETRIC ROLL IN SHIPS: FROM MATHIEU TONGUES TO ATTRACTION BASINS

Dumitru DELEANU [1] & Simona-Ana SÎRBU [2,3]

[1] Constanta Maritime University, Faculty of Marine Engineering, 104 Mircea cel Batran Street, 900663, Constanta, Romania, e-mail address: dumitrudeleanu@yahoo.com
[2] Constanta Maritime University, Faculty of Marine Engineering, 104 Mircea cel Batran Street, 900663, Constanta, Romania, ORCID ID 0009-0006-0071-8874, e-mail address: simona.sirbu@cmu-edu.eu
[3] National University of Science and Technology Politehnica Bucharest, Doctoral School of Entrepreneurship, Engineering and Business Management, 313 Splaiul Independentei Street, 060042, Bucharest, Romania

Abstract: Parametric roll is a nonlinear ship-motion instability triggered when the encounter frequency approaches twice the natural roll frequency, causing periodic modulation of restoring moment and possible amplification to large roll angles. This paper develops and exploits a compact, one-degree-of-freedom roll model to numerically detect the principal nonlinear phenomena associated with parametric roll in a modern containership. The model combines a fifth-order polynomial restoring lever, a composite damping with linear, quadratic, cubic and smoothed Coulomb terms, and a parametric modulation of the linear restoring. Starting from the dimensionless parametric roll equation, three diagnostic products are obtained: (i) Ince-Strutt diagram showing the main Mathieu tongue; (ii) basins of attraction that quantify sensitivity to initial conditions and "escape" to extremely large roll angles; (iii) frequency-response curves that expose jumps and hysteresis loops. From an operational point of view, the diagrams show where amplification of roll motion is likely, the basins identify which perturbations lead the ship into a dangerous situation, and the frequency-response/hysteresis curves indicate how transitions occur and how persistent they are. Such tools can guide both ship design as well as the decisions needed during navigation (speeds/courses that avoid critical encounter bands). To make numerical simulation more applicable, we calibrate the model parameters to a representative containership.
Key words: Attraction basin, Instability tongue, Ship parametric rolling.

1. INTRODUCTION

Parametric roll is a nonlinear instability that can drive large roll angles in otherwise modest sea conditions. It arises when the ship's restoring characteristics vary periodically with the encounter of waves, most often in head or following seas, so that the roll dynamics experience an effective parametric excitation near twice the natural roll frequency.

Under such conditions, even small external perturbations can be amplified cycle by cycle, producing sudden growth, large steady oscillations, or strongly modulated responses that challenge the vessel's operational limits.

Despite the fact that this phenomenon has been studied for decades using Mathieu-Hill-Duffing models, there remains a practical need for numerical tools and maps that make the onset and saturation of parametric roll readily identifiable for concrete ship classes and operating points [1 – 2, 5 - 9].

The present paper adopts a numerical-centric perspective to systematically explore interesting nonlinear phenomena associated with parametric roll in ships. Using a compact parametric rolling model in which the parameter values are representative of a classical containership, we focused on three clear and reproducible geometric tools: the main Mathieu tongue, basins of attraction, and frequency-response curves. All simulations employ transient and stationary windows where the peak roll amplitudes are measured.

Escape criteria are defined by angle thresholds motivated by operational practice.

This protocol enables like-for-like comparison across different parameter values.

In future research, we will replace the polynomial restoring moment approximation with tabulated hydrostatic data and the idealized sinusoidal sea forcing with stochastic sea-state excitation to achieve a more realistic representation of the parametric roll phenomenon.

Journal of Marine Technology and Environment
DOI:10.53464/JMTE.02.2026.02
ISSN (Print): 1844-6116
ISSN (Online): 2501-8795
https://www.jmte.eu

2. NONLINEAR PARAMETRIC ROLL EQUATION

We denote the roll angle by $\phi(t)$, with $\dot{\phi}$ and $\ddot{\phi}$ its time derivatives. The nonlinear equation of parametric roll in general form reads:
where:

$$I_{eff}(\phi) \cdot \ddot{\phi} + D(\dot{\phi}) + R(\phi, t) = 0 \qquad (1)$$

- $I_{eff}(\phi) = I_\phi + \delta I_\phi + A\phi^2$ is the effective moment of inertia about the roll axis. Here, I_ϕ is the ship moment of inertia, δI_ϕ the moment of inertia of the added mass of surrounding water, and $A\phi^2$ is weakly amplitude-dependent (it is optional and set to zero in the core results).
- $D(\dot{\phi}) = D_1\dot{\phi} + D_2|\dot{\phi}|\dot{\phi} + D_3\dot{\phi}^3 + D_C\, sgn(\dot{\phi})$ is the nonlinear composite damping moment. D_1, D_2, and D_3 are constants that capture linear, quadratic, and cubic viscous effects, while $D_C\, sgn(\dot{\phi})$ is a smoothed Coulomb term that regularizes dry friction near $\dot{\phi} = 0$. For numerical reasons, it is replaced by $D_C\, tanh(\dot{\phi}/\varepsilon)$, with $\varepsilon \ll 1$.
- $R(\phi, t) = \rho g \nabla [GZ_{stat}(\phi) + GZ_{par}(\phi, t)]$ represents the restoring moment. Here, ρ is the water density, g the gravitational acceleration, ∇ the mass displacement, $GZ_{stat}(\phi)$ the static lever, and $GZ_{par}(\phi, t)$ the contribution of the parametric excitation. The static lever can be approximated by an odd polynomial $GZ_{stat}(\phi) = K_1\phi + K_3\phi^3 + K_5\phi^5$, where $K_1 \approx GM_m$ (constant part of metacentric height), $K_3 < 0$ and $K_5 > 0$ capture softening and saturation, respectively. The periodic variation of the restoring moment induced by longitudinal waves mainly affects the linear part, $GZ_{par}(\phi, t) = (GM_a\, cos\omega_e t) \cdot \phi$, where ω_e denotes the wave encounter frequency and GM_a is the variable part of the metacentric height.

Remark: Some external and bias moments can be introduced in (1). External forcing arises from the small direct roll excitation caused by asymmetry and by diffracted waves. Bias moments can be associated with a constant heel due to wind or cargo shift. Although these moments do not cause instability, they can trigger or amplify it (especially by shifting the equilibrium to an angle $\phi \neq 0$) [3, 4].

The small-angle ship's natural frequency, ω_ϕ, is provided by:

$$\omega_\phi = \sqrt{\frac{\rho g \nabla GM_m}{I_\phi + \delta I_\phi}}$$

Let $\tau = \omega_\phi t$, $x(\tau) = \phi(t)$, $(\cdot)' = d(\cdot)/d\tau$. Dividing (1) by I_{eff} and noting that $d/dt = \omega_\phi d/d\tau$ and $d^2/dt^2 = \omega_\phi^2 d^2/d\tau^2$, yields the nondimensional form of the parametric roll equation:

$$x'' + d_1 x' + d_2|x'|x' + d_3(x')^3 + d_C\, tan(x'/\tilde{\varepsilon}) + \qquad (2)$$
$$+[1 + \mu\, cos(\sigma\tau)]x + k_3x^3 + k_5x^5 = 0$$

where the dimensionless coefficients are:

$$d_1 = \frac{D_1}{(I_\phi + \delta I_\phi)\omega_\phi}, d_2 = \frac{D_2}{I_\phi + \delta I_\phi}, d_3 = \frac{D_3\omega_\phi}{I_\phi + \delta I_\phi},$$

$$d_C = \frac{D_C}{(I_\phi + \delta I_\phi)\omega_\phi^2}, \tilde{\varepsilon} = \frac{\varepsilon}{\omega_\phi}, \mu = \frac{GM_a}{GM_m}, \sigma = \frac{\omega_e}{2\omega_\phi},$$

$$k_3 = \frac{K_3 \cdot \rho g \nabla}{(I_\phi + \delta I_\phi)\omega_\phi^2}, k_5 = \frac{K_5 \cdot \rho g \nabla}{(I_\phi + \delta I_\phi)\omega_\phi^2} \qquad (3)$$

This nondimensionalization makes explicit that the linear restoring scales as unity, the static nonlinearity is governed by (k_3, k_5), and the parametric excitation enters as $\mu\, cos(\sigma\tau)$.

3. VESSEL-SCALE PARAMETRIZATION

We adopt a coherent parametric set representative of a modern ~8000 TEU container ship. These values are used throughout unless stated otherwise (see Table 1).

Table 1. The containership dimensional parameters

Parameter	Value	Unit
I_ϕ	$1.4014 \cdot 10^{10}$	$kg \cdot m^2$
δI_ϕ	$2.17 \cdot 10^9$	$kg \cdot m^2$
D_1	$3.5393 \cdot 10^8$	$kg \cdot m^2/s$
D_2	$1.8826 \cdot 10^8$	$kg \cdot m^2$
D_3	$1.1232 \cdot 10^8$	$kg \cdot m^2 \cdot s$
D_C	$7.4361 \cdot 10^5$	$kg \cdot m^2/s^2$
ε	0.002	$1/s$
ρ	1000	kg/m^3
∇	76468	m^3
$K_1 \approx GM_m$	1.91	m
K_3	-3.96	m
K_5	2.64	m

Journal of Marine Technology and Environment
DOI:10.53464/JMTE.02.2026.02
ISSN (Print): 1844-6116
ISSN (Online): 2501-8795
https://www.jmte.eu

With these values, one has $\omega_\phi = 0.2975\, rad/s$, and $T_\phi = 2\pi/\omega_\phi = 21.12\ s$. Additionally, from (3), the following no dimensional parameters are obtained:

$$d_1 = 0.0736, d_2 = 0.0116, d_3 = 0.0021, d_C = 0.0005,$$

$$\tilde{\varepsilon} = 0.0067, k_3 = -2.0763, k_5 = 1.3842.$$

4. NUMERICAL SIMULATIONS

In every simulation, we integrated the non-dimensional roll equation (2) with an explicit, adaptive Runge-Kutta method using relative and absolute tolerances of 10^{-6} and 10^{-8}. The maximum internal step size was $\Delta\tau_{max} = 0.05$. The running time was split into two equal intervals representing transitory and stationary windows. Unless otherwise stated, the initial conditions correspond to a small perturbation, $\phi(0) = 0.2^0, \dot{\phi}(0) = 0$.

4.1 Single-case dynamics

We first simulated the ship's behaviour in the vicinity of the resonance condition $\omega_e \approx 2\omega_\phi$ to determine the rate of increase of the initial disturbance $\phi(0)$. Figure 1a presents the time histories of ship roll angle for $\omega_e = 0.6055$ (meaning σ = 1.0193 and μ = 0.4) and GM_a = 0.764. An exponential increase in roll oscillations is evident. With a running time of 800 s, the values 23.4° and 19.8° were found for the amplitudes of the transient and stationary phases, respectively. A not-very-consistent "departure" from the theoretical resonance point has the opposite effect. The initial perturbation, even of the order of a few degrees, is "annihilated" by the ship's damping (see Fig. 1b, obtained for σ = 1.076 and ϕ (0) = 2°).

Between the two situations described above, a transition process occurs in which the dangerous roll oscillations develop increasingly more slowly. Thus, for σ = 1.055, at 800 s after the oscillation's initiation, the ϕ angle was only 2°. It reached the maximum value of 14° for t ~1100 s and stabilized at 12.5° (see Fig. 1c).

Similar to chaotic dynamical systems, the initial conditions can play a decisive role in the ship's final response. For example, by choosing σ = 1.0796 and ϕ(0) = 1.8508703°, the ship is subjected to a minor rolling of 0.87° for no less than 4000 s, after which a jump occurs to another permanent state characterized by a moderate rolling of 6.5° (see Fig. 1d). Just an infinitesimal shift to ϕ (0) = 1.8598702°, results in a long period with ϕ max = 0.9° followed by a decay to 0°.

In conclusion, two parameters that require great attention when issuing a judgment are the tracking time of the ship's behavior and the starting conditions.

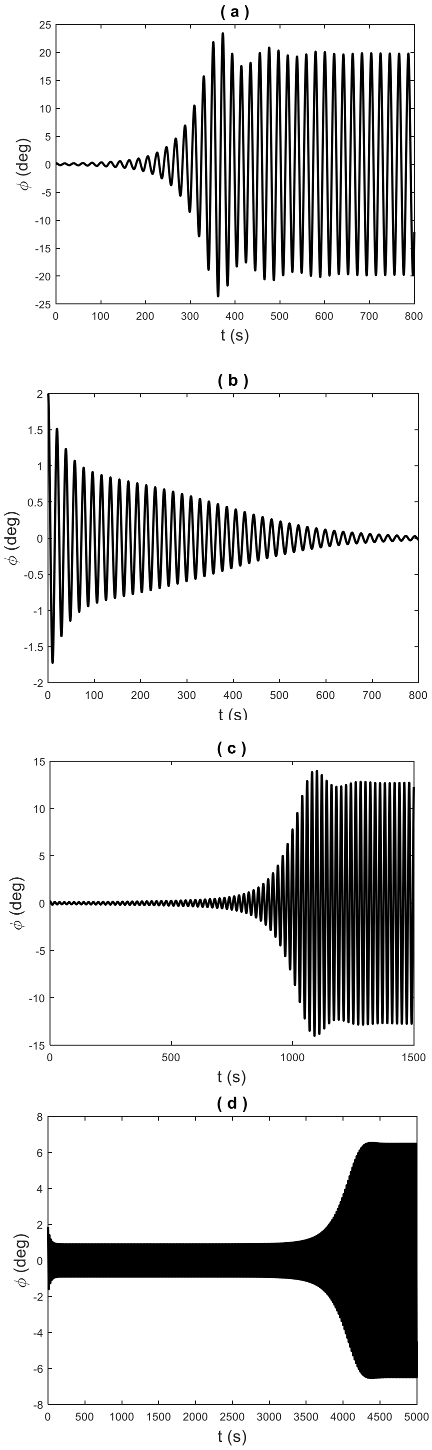

Figure 1 Time histories of ship roll angle

where:
(a) σ = 1.0193, ϕ (0) =0. 2°; (b) σ = 1.076, ϕ (0) = 2°; (c) σ = 1.055, ϕ (0) =0. 2°; (d) σ = 1.0796, ϕ (0) =1.8508703°.

4.2 The principal Mathieu's tongue

Journal of Marine Technology and Environment
DOI:10.53464/JMTE.02.2026.02
ISSN (Print): 1844-6116
ISSN (Online): 2501-8795
https://www.jmte.eu

As expected from Mathieu-type theory, there exists a single dominant V–shaped tongue with a rounded tip centred near σ = 1 in the (σ, μ) plane. It corresponds to the combinations (σ, μ) of parameters associated with the longitudinal waves for which the small initial perturbation is abruptly amplified.

To represent it, we scan over a rectangular grid with 101 × 101 uniformly distributed points. For each pair (σ, μ), we recorded the peak amplitude $A_{max} = max|\phi(t)|$ in the stationary stage and amplitude class. The latter could be 1 if $A_{max} \leq 2°$, 2 if $2° < A_{max} \leq 10°$, 3 if $10° < A_{max} \leq 20°$, 4 if $20° < A_{max} \leq 30°$, and 5 otherwise. Figures 2 to 4 report our findings for running times in the ranges [0, 400] s, [400, 800] s, and [1500, 3000] s. A first remark is easy to intuit from the analysis of these figures. A sufficiently long observation is needed for the full formation of the instability tongue and the separation into amplitude classes within it.

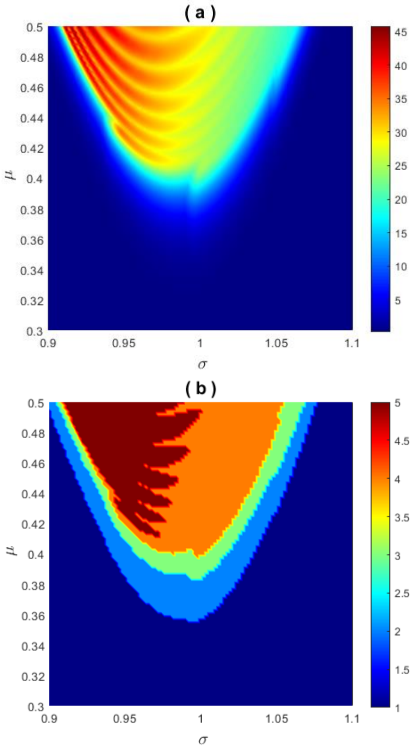

Figure 2 The main instability tongue case I.

The colour bar shows the peak roll amplitude (a) or amplitude class (b).

The running dimensional time *t* was in the range [0, 400] s.

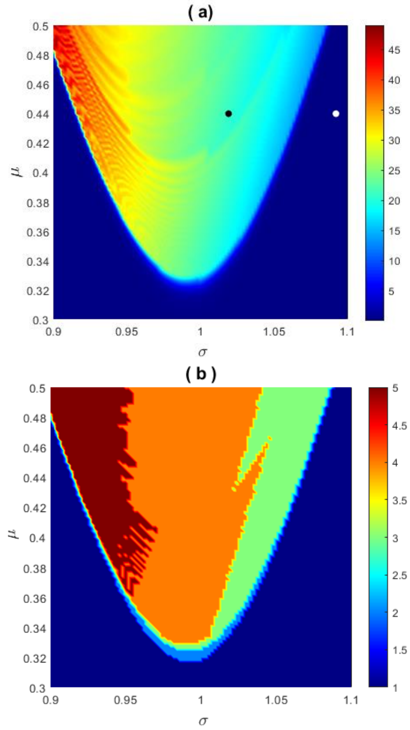

Figure 3 The main instability tongue-case II .

The same as in Fig. 2, but the running time was in the range [400, 800] s.

The black and white points correspond to the time series presented in Figs. 1a, b.

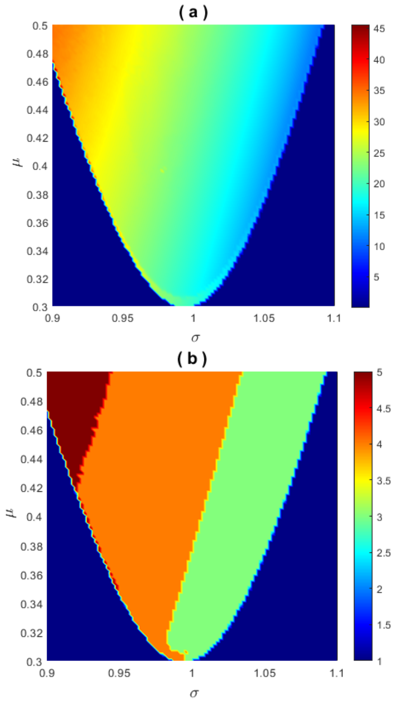

Figure 4 The main instability tongue-case III

Journal of Marine Technology and Environment
DOI:10.53464/JMTE.02.2026.02
ISSN (Print): 1844-6116
ISSN (Online): 2501-8795
https://www.jmte.eu

The same as in Fig. 2, but the running time was in the range [1500, 3000] s.

This division into classes is extremely pronounced, with amplitudes that increase as σ decreases and μ increases. If the (σ, μ) point falls inside the colored tongue, a parametric amplification of the roll angle to a saturated level is expected. Conversely, if the (σ, μ) point lies outside the tongue, any initial perturbation should decay to zero or to very small oscillations. Near the tongue's tip and on its left side, jump phenomena and path dependence are expected. Local grid refinement in these areas reveals fine structures in which large-amplitude branches coexist with moderate-amplitude branches (see Fig. 5).

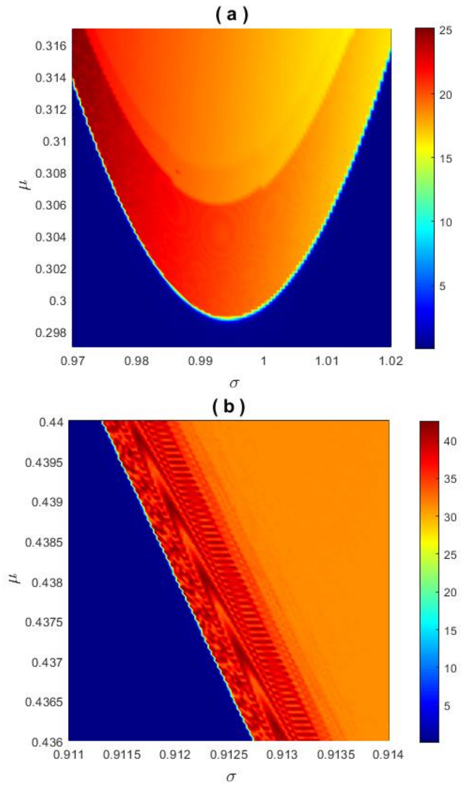

Figure 5 Extracts from Fig. 4a that highlight either jump phenomena or coexistence of different amplitude classes in an extremely small region

We have already highlighted the importance of choosing a sufficiently long observation (running) time to minimize decision-making errors. In addition, Figure 6 shows the variation in the percentages of the five amplitude classes as a function of running time in the two collection windows: the transient and the stationary. We can see that 3000 – 4000 seconds are necessary and sufficient for stabilization. For this reason, the following simulations will use a time that balances efficiency and the correctness of the conclusions: T_{run} = 3000 s.

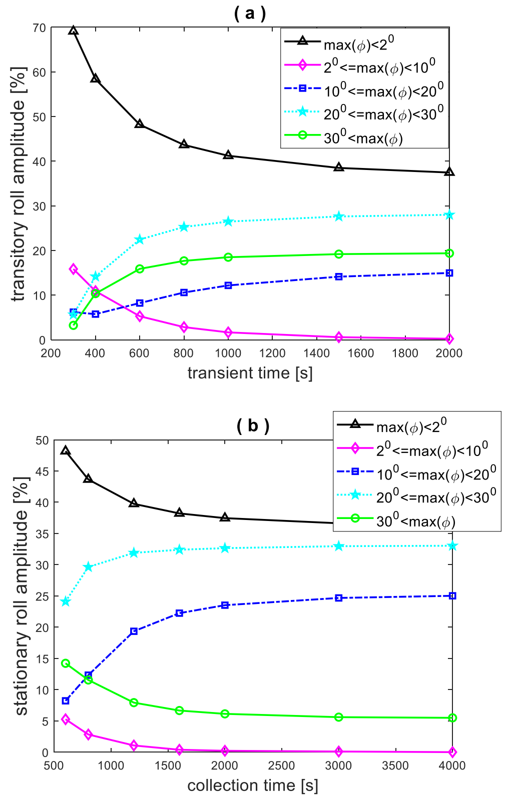

Figure 6 The dependence of the percentage of each amplitude class on running time in
(a) transitory window; (b) stationary window

Up to this point we have used the values set in Section 3 for the system's parameters. Let us now identify the effects of changing the most important of them.

As the small-amplitude damping coefficient d_1 is raised, the tip of Mathieu's tongue moves toward higher μ. Therefore, in the previously used domain (σ, μ) a significant increase in the percentage of amplitude class 1 and a decrease of classes 3, 4 and 5 is observed (see Fig. 7a). In addition to the decrease in the steady state amplitude, there is also a delay in the development of the parametric roll, which allows the crew to take the necessary measures (see Fig. 7b). Increasing the nonlinear damping coefficients d_2 and d_3 reduces slightly the saturated amplitude without substantially altering the initial onset.

Journal of Marine Technology and Environment
DOI:10.53464/JMTE.02.2026.02
ISSN (Print): 1844-6116
ISSN (Online): 2501-8795
https://www.jmte.eu

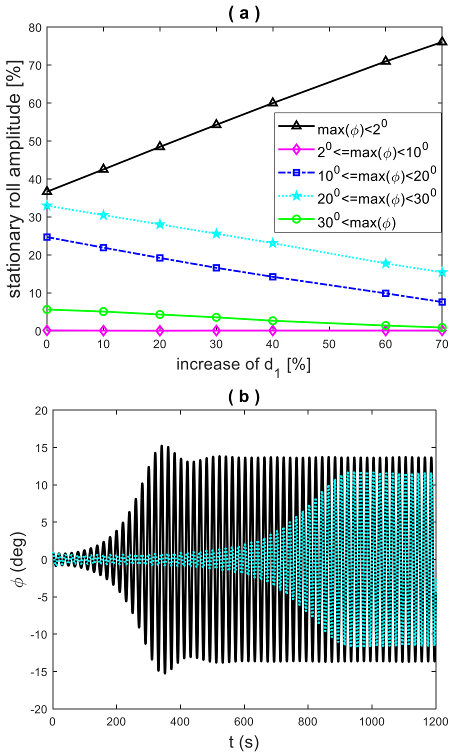

Figure 7 (a) Effect of increasing damping coefficient d_1 on the steady state amplitude;
(b) Time histories of roll angle for μ = 0.4, σ = 1.05, φ (0) = 1° and d_1 = 0.0736 (black) or d_1 = 0.1104 (green)

An increase in the softening coefficient k_3 does not change the position of the instability zone in the (σ, μ) plane, but within Mathieu tongue a beneficial shift occurs from amplitude classes 4 and 5 to class 3 (see Fig. 8a). At least for the combination of parameters chosen in the paper, a modification of k_5 does not seem to influence significantly the weights of the amplitude classes (see Fig. 8b).

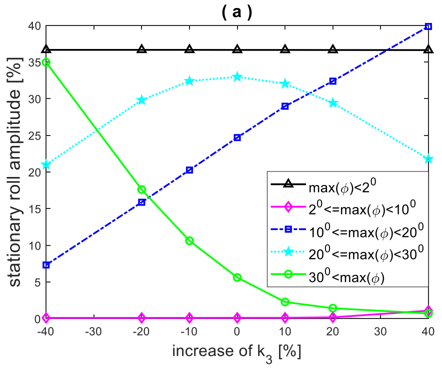

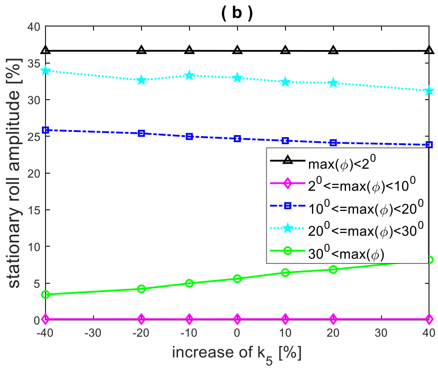

Figure 8 Influence of restoring nonlinearities on the stationary roll amplitudes

We suggested in Fig. 1d a possible factor with a major effect on the ship’s response to rolling: the initial conditions. If a small disturbance is more easily attenuated by the ship’s damping, it is possible that more severe initial conditions will help the development of parametric roll in a much shorter time and at a significantly reduced wave height (decreased μ). Indeed, compared with Fig. 4b, the two panels of Fig. 9 show a minor reconfiguration within the instability zone, but a shift of the tip toward much lower values of μ (which is undesirable).

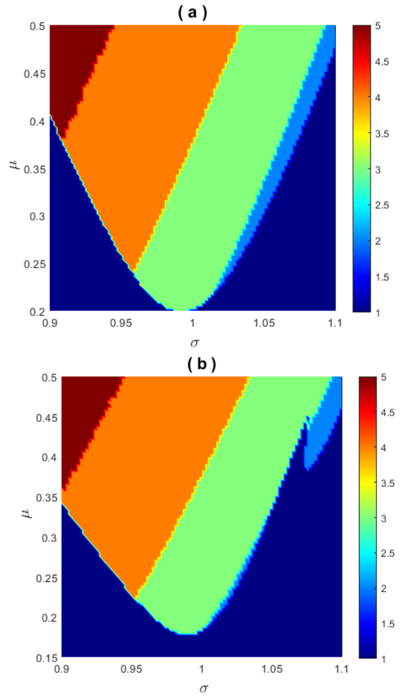

Figure 9 Shifting effect of the initial conditions on the Mathieu tongue

(a) φ (0) = 2°, dφ/dt (0) = 0;
(b) φ (0) = 5°, dφ/dt (0) = 1°/s

4.3 Basins of attraction

Journal of Marine Technology and Environment
DOI:10.53464/JMTE.02.2026.02
ISSN (Print): 1844-6116
ISSN (Online): 2501-8795
https://www. jmte.eu

Attractor basins are computed in the ($\phi(0)$, dϕ/dt (0)) plane by integrating the roll equation (2) from a Cartesian grid of 101 x 101 initial states over a running time T = 3000. Each trajectory is assigned an amplitude class, as described in the previous section.

For the container ship parametrization presented in Section 3, near the principal resonance σ = 1 and moderate modulation μ, the basin portrait exhibits a safe neighbourhood around the origin $\left(\phi(0)=0, \dot{\phi}(0)=0\right)$ where curved bands associated with amplitude classes 1 and 2 intertwine in a seemingly complicated way. Somewhere farther from the origin (a few-degree zone), two or more thin lobes of large response, roughly aligned with the vertical axis, can be observed. A local focus on the boundary between low- and high-amplitude classes reveals a fringed boundary with very thin bands of medium amplitude. For large $\phi(0)$, escape pockets at the corners of the analyzed domain can be detected (see Fig. 10a). With the increase of μ, this picture changes substantially in the sense that small classes disappear and are replaced on an increasingly larger area of the ($\phi(0)$, μ) plane by zones that pose a major risk for ship safety (see Fig. 10b). Far from resonance, we might think that for a fixed μ the small amplitude classes expand and the others retreat. This is true for μ > 1 (see Fig. 10d) but not otherwise. Looking again at Fig. 4b, we can understand that the area of high amplitudes is concentrated to the left of the typical value σ = 1. Here, taking into account the initial disturbances, we can only expect high-amplitude classes (see Fig. 10c).

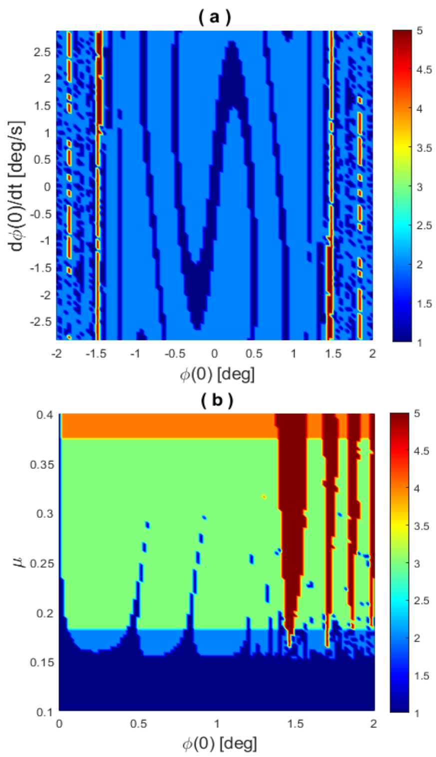

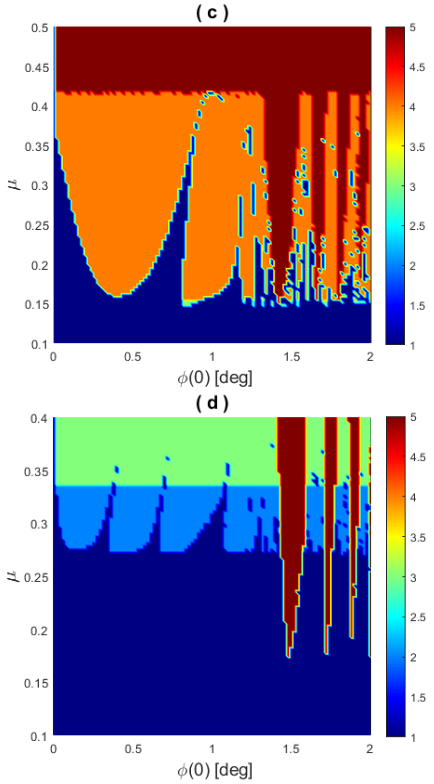

Figure 10 Basins of attraction for different amplitude classes

where
(a) for σ = 1 and μ = 0.178;
(b) Sensitivity of amplitude classes on φ (0) and μ for σ = 1;
(c) The same but for σ = 0.92 (c) or σ = 1.05 (d).

Regarding the influence of the main parameters on the basin's geometry, we can summarize the following:

- Increasing d_1 expands the small-amplitude basin and decreases the others slowly. The large-amplitude lobes are pushed outward. This tendency is strongest near σ = 1 and moderate μ (see Figs. 11a and 12a).

- Stronger k_3 enlarges small amplitudes basins in the (φ (0), μ) plane but introduces a lot of very fringed zones of large amplitude for φ (0) > 1° or μ > 0.35 (see Fig. 12b). For fixed μ and σ = 1, the ship's situation is better because a transfer from amplitude class 3 to class 2 is observed (see Fig. 11b).

Journal of Marine Technology and Environment
DOI:10.53464/JMTE.02.2026.02
ISSN (Print): 1844-6116
ISSN (Online): 2501-8795
https://www.jmte.eu

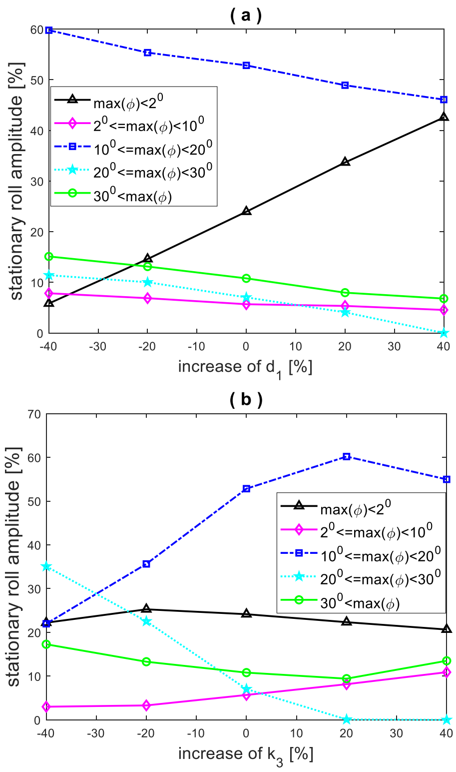

Figure 11 The dependence of the attraction basin of each amplitude class of (a) d_1; (b) k_3

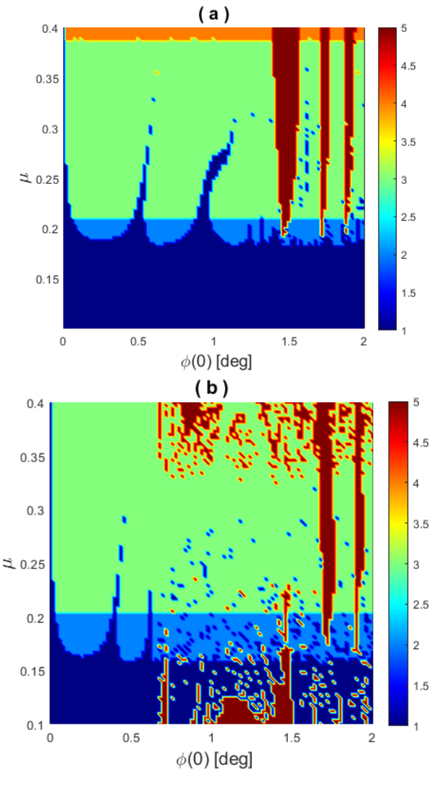

Figure 12 The dependence of amplitude classes on φ (0) and μ for σ = 1:

(a) an increase of d_1 by 20%; (b) an increase of k_3 by 40%

4.4 Frequency – response curves

These curves present the steady peak amplitude as a function of frequency ratio σ for a given set of vessel parameters. Unlike the synchronous roll, where these curves have the shape of Ω letter, with the upper part more or less pointed and inclined to one side, in this case their appearance is trapezoidal (see Fig. 13a). For a fixed modulation depth μ, the damping manages to "extinguish" the initial disturbance except for an interval [σ_{min}, σ_{max}] approximately centred on σ = 1 at the ends of which a jump up and down in the value of oscillation amplitude occurs. The length of this interval increases with μ, as does the roll amplitude. Of interest are the sharp peaks at the ends of the interval, which indicate major transformations in the ship's behaviour resulting from small changes in wave encounter frequency or the ship's natural roll frequency. The same type of response is obtained by tightening the initial conditions for a fixed μ, with the observation that, in the interval of non-zero amplitude, the curves are superimposed (see Fig. 13b).

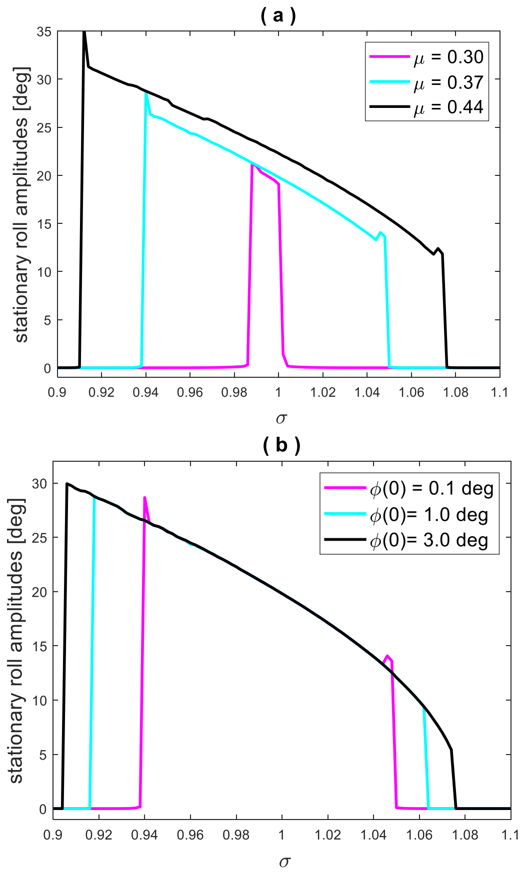

Figure 13 Frequency – response curves for (a) three different μ; (b) three different φ (0) and μ = 0.37

Augmenting the linear drag coefficient d_1 has the expected positive effect, namely narrowing the interval

Journal of Marine Technology and Environment
DOI:10.53464/JMTE.02.2026.02
ISSN (Print): 1844-6116
ISSN (Online): 2501-8795
https://www. jmte.eu

[σ_{min}, σ_{max}] but not the stationary roll amplitude (only to a small extend; see Fig. 14a). Doing the same but for restoring coefficient k_3, we obtained an opposite effect: preserving the dangerous frequency σ range but decreasing the roll amplitudes as k_3 increases (see Fig. 14b). Somehow similar effects are produced by changing other parameters, for example k_5 and d_c (see Figs. 14c, d).

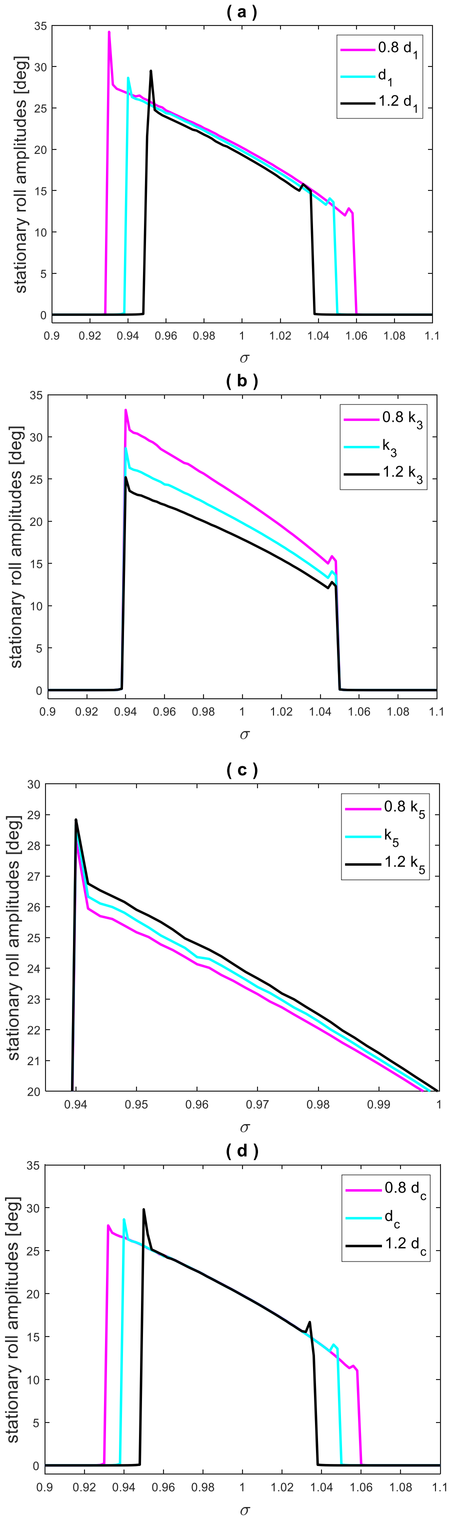

Figure 14 Frequency – response curves for μ = 0.37

and:
(a) Three linear damping coefficients; (b) Three softening restoring coefficients; (c) Three saturation restoring coefficients; (d) Three Coulomb damping coefficients

4.5 *Effects of GM_m and frequency detuning*

We close this numerical study with a brief presentation of the influence of the constant part of metacentric height, GM_m, on the ship's response. Varying GM_m shifts ω_ϕ and therefore the horizontal placement of the Mathieu tongue when plotted versus σ (for unchanged ω_e). A moderate increase of GM_m generally reduces the likelihood of parametric roll. However, excessively large GM_m does not eliminate parametric instability and may even exacerbate dynamic loads and roll accelerations, merely relocating the resonance rather than suppressing it (see Fig. 15).

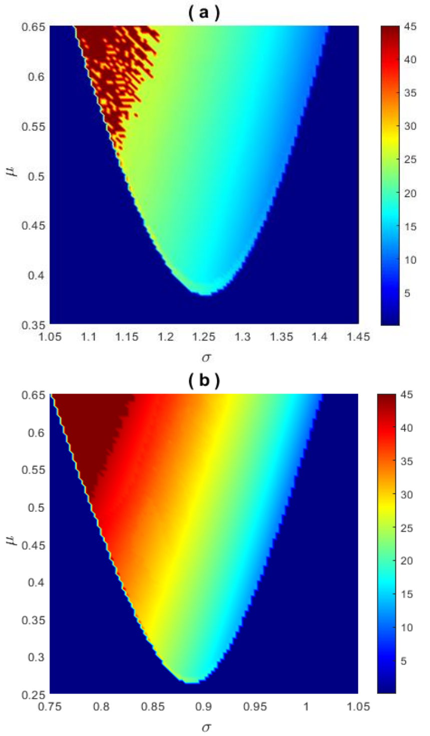

Figure 15 The main Mathieu tongue for (a) GM_m = 1.2; (b) GM_m = 2.4.
The colorbar shows the stationary roll amplitudes

5. CONCLUSIONS

In the paper, we employed a nonlinear Duffing-Mathieu roll oscillator with composite viscous/Coulomb damping and a high-order polynomial restoring lever to

Journal of Marine Technology and Environment
DOI:10.53464/JMTE.02.2026.02
ISSN (Print): 1844-6116
ISSN (Online): 2501-8795
https://www. jmte.eu

obtain clear numerical bifurcation/instability maps, attraction basins, and frequency-response curves for an ~8000 TEU containership. Such maps can guide both ship design (damping devices, GM tuning, etc.) and operations (speed/course choices that affect wave encounter frequency). Limitations of the model (single-degree-of-freedom, polynomial law for GM, sinusoidal sea forcing) are explicit and indicate where the model should be further developed.

Within this scope, we found that:

Onset of parametric roll near the main Mathieu tongue is governed by μ relative to σ, but composite damping and softening shift and shape the instability region;

Basins of attraction expose regions in $\left(\phi(0), \dot{\phi}(0)\right)$ plane where small impulses can trigger large roll amplitudes despite unchanged mean conditions. Additionally, their aspect can be very complicated;

The shape of the frequency-response curves is practically trapezoidal, in obvious contrast to the synchronous roll. The transition from small amplitudes to truly dangerous ones occurs suddenly with small variations of σ and depends on damping components, initial conditions, and modulation depth.

6. CREDIT AUTHORS STATEMENT

Conceptualization: D.D.

Data curation: S-A.S.

Formal analysis: D.D.

Funding acquisition: S-A.S.

Investigation: D.D.

Methodology: D.D.

Project administration: D.D.

Resources: D.D., S-A.S.

Software: D.D., S-A.S.

Supervision: D.D.

Validation: D.D.

Visualization: S-A.S.

Writing – original draft: D.D., S-A.S.

Writing – review & editing: S-A.S..

7. REFERENCES

[1] Azimi M., (2022), Stability and bifurcation of Mathieu-Duffing equation, *Int. J. of Non-linear Mechanics*, vol. 144, DOI 10.1016/j.ijnonlinmec.2022.104049.

[2] Carmel S.M., (2006), Study of parametric rolling event on a Panama container vessel, *Journal of the Transportation Research Board*, vol. 1964, 56 – 63, DOI 10.1177/0361198106196300108.

[3] Deleanu D., Dumitrache C.L., (2019), Numerical study of a container ship model for the uncoupled parametric rolling, *IOP Conf. Ser.: Mater. Sci. Eng.* 591 012106, DOI 10.1088/1757-899X/591/1/012106.

[4] Deleanu D., Dumitrache C.L., (2020), Controlling the parametric roll of a container ship model by changing the forward velocity, *IOP Conf. Ser.: Mater. Sci. Eng.* 916 012024, DOI 10.1088/1757-899X/916/1/012024.

[5] Galeazzi R., Blanke M., Poulsen N.K., (2013), Early detection of parametric roll resonance on containerships, *IEEE Transactions on Control System Technology*, vol. 21(2), 489-503, DOI 10.1109/TCST.2012.2189399.

[6] Ghemari I, Faltinsen O.M., Greco M., (2015), Investigation of parametric resonance in roll for container carrier ships, *Proceedings of the ASME International Conference on Ocean, Offshore and Arctic Engineering*, St. John's, Newfoundland, Canada, DOI 10.1115/OMAE2015-41528.

[7] Holden Ch., Galeazzi R., Rodriguez C., Perez T., Fossen T.I., Blanke M., Santos Neves M.A., (2007), Nonlinear containership model for the study of parametric roll resonance, *Modelling, Identification and Control*, vol. 28(4), 87-103, DOI 10.4173/mic.2007.4.1.

[8] Kovacic I., Rand R., Sah S.M., (2018), Mathieu's equation and its generalizations: Overview of the stability charts and their features, *Applied Mechanics Reviews*, vol. 70(2): 020802, DOI:10.1115/1.4039144.

[9] Paulling J.R., (2011), Parametric rolling on ships. Then and now. Contemporary ideas on ship stability and capsizing in waves, *Fluid Mechanics and its Applications*, vol. 97, 253-266, DOI:10.1007/978-94-007-1482-3-19.